Extreme Variability of the Tropical Tropopause over the Indian Monsoon Region

Vanmathi Annamalai and Sanjay Kumar Mehta*

[1] Research Institute, SRM University, Kattankulathur, Chennai, Tami Nadu, India

*Corresponding author: Sanjay Kumar Mehta (ksanjaym@gmail.com)

Key Points:

- Proposed a method to identify the extreme variability such as the coldest, warmest, highest and lowest tropopauses
- The coldest tropopause is found to be sharper while the warmest, highest and lowest tropopauses are broader.
- Possible mechanisms such as equatorial wave propagation, deep convection and ozone transport are examined.

Abstract

The extreme variability of the cold point tropopause temperature (T_{CPT}) and height (H_{CPT}) are examined over a tropical station, Gadanki (13.45^o N, 79.2^o E) using high-resolution radiosonde data during the period 2006-2014. The extreme variabilities such as the coldest (warmest) tropopause is defined if T_{CPT} is lesser (greater) than the lower (upper) limit of its two-sigma level whereas the highest (lowest) tropopause is defined as the H_{CPT} is greater (lesser) than the lower (upper) limit of its two-sigma level. In total 161 extreme cases such as the coldest (52) and warmest (30) T_{CPT} and the highest (57) and lowest (22) H_{CPT} are observed. The coldest (187.2±1.60 K, 17.3±0.52 km), warmest (194.2±1.78 K, 16.9±0.89 km), lowest (191.7±1.78 K, 18.2±0.55 km) and highest (191.8±2.11 K, 16.2±0.38 km) occurs without preference of season. These extreme tropopause cases occur independently. Thermal structure of the coldest tropopause cases reveals that they are often sharper whereas the warmest, highest and lowest tropopause are broader. Water vapor and ozone concentrations are found to be high for the warmest tropopause and low for the coldest tropopause. Under the shallow convection, extreme temperature profiles, in general, show prominent warming between 8-14 km while anomalous cooling (warming) just below (above) the CPT. The occurrence of the tropical cyclones, cirrus clouds and equatorial wave propagation are the possible candidates for the occurrence of the extreme tropopauses.

Plain Language Summary

On day-to-day scale, cold point tropopause (CPT) height (H_{CPT}) and temperature (T_{CPT}) sometimes varies extremely which is generally ignored partly due to its rare occurrence and partly due to complex UTLS processes. The long-term observations of the radiosonde data provided us with an opportunity to collect the sufficient number of extreme tropopause cases

identified as the cases falling outside the two-sigma level of climatological mean tropopause over the period 2006-2014.. In contrary to generally accepted concept that the tropopause is higher and colder during northern winter and lower and warmer tropopause during northern summer, finding from this report indicate that the higher tropopause may not be always colder one and lower tropopause may not be always warmer one. Four different class of the thermal structure of the tropopause exist in the tropical atmosphere which is classified based on the occurrence of the colder, warmer, higher and lower tropopause. Possible mechanisms responsible for such extreme variabilities such as equatorial wave propagation, deep convection, water vapor and ozone transport are examined.

1 Introduction

The tropospheric temperature is maintained by convective and radiative (e.g., water vapor cooling) processes while the stratospheric temperature is mainly driven by radiative processes (e.g., ozone heating). Thus, tropopause as the boundary between troposphere and stratosphere forms in response to achieve the radiative-convective equilibrium. Though tropopause acts as a lid on the troposphere and hence provides a physical barrier for the stratosphere-troposphere exchange (STE) process (Holton et al., 1995) it is the gateway for the stratospheric water vapor. Dynamical processes such as deep convection (thunderstorms and cyclonic activities), planetary wave propagation, sudden stratospheric warmings (SSW) not only promote STE processes but also causes extreme tropopause variabilities. However, how extreme are these processes and how extremely the tropopause respond to them, is not known. The tropopause may be extremely cold, warm, high and low. For example, the formation of the coldest tropopause has a direct bearing to the low water vapor in the lower stratosphere and hence it controls the stratospheric chemistry by protecting the ozone destructions (Fueglistaler et al., 2009).

Observations of the temperature profiles in the upper troposphere and lower stratosphere (UTLS) region reveal a variety of structures such as broad tropopause, sharp tropopause and multiple tropopauses. Spatial variability of the tropopause indicates that the broader tropopause mainly occurs over the region of the subsidence and they are generally warmer (Kim & Son, 2012; Schmidt et al., 2004; Seidel et al., 2001). Whereas sharper and colder tropopause generally occurred over the region of the active convection center. Multiple tropopauses form due to planetary wave activities, circus clouds occurrence and horizontal advection (Añel et al., 2008; Mehta et al., 2011; Reid & Gage, 1996). Several studies have been carried out on the variability of the tropopause on different time scales ranging from the diurnal scale (hourly variations) to long-term variations linking to various atmospheric processes such as non-migrating tides for diurnal variabilities, convection and planetary wave activities for sub-daily and day to day variations, tropospheric convection and stratospheric Brewer-Dobson circulation for seasonal and annual variations, quasi-biennial oscillations (QBO), El Nino Southern Oscillation (ENSO) solar cycle and volcanic activities for interannual variabilities and increase in greenhouse gases for long-term variabilities. The cold point tropopause (CPT) temperature changes ~ ±0.5 K due to QBO (Randel et al., 2003; Schmidt et al., 2004).

Convection plays a dominant role in the tropopause variability. Generally, the tropopause found to be at lower altitude during deep convection events (Mehta et al., 2010; Muhsin et al., 2018). However, during the overshooting convection tropopause can occur at extremely high altitude and moist air can even intrude into the lower stratosphere. These rare convective overshoots followed by strong downdraft can weaken the stability of the TTL region (Kumar, 2006). Such stratospheric intrusions leave the signature of high ozone concentrations and low relative humidity.

Several studies have been carried out on the tropical tropopause using high-resolution radiosonde data (Jain et al., 2011; Mehta et al., 2010; Sunilkumar et al., 2013), reanalysis data (Highwood & Hoskins, 1998; Randel et al., 2000) and satellite measurement (J. Kim & Son, 2012; Mehta, Ratnam, & Krishna Murthy, 2011; Ratnam et al., 2005). By using the Radiosonde data, Sunilkumar et al. (2013) shown that the negative correlation between the CPT temperature and height indicate that it is mainly dominated by the stratospheric process while positive correlation means the CPT is dominated by the surface or tropospheric process (Shepherd, 2002). Thus, variability in the cold point is found to explain much of the variability in lower-stratospheric water vapor concentrations (Fueglistaler & Haynes, 2005; Gettelman et al., 2010). In tropics, convection is the prime factor which modulates the tropopause, together with, Kelvin waves planetary scales and Rossby waves also could modulate the tropopause (Jain et al., 2006; Matsuno, 1966) and the trace gases which is entering to lower stratosphere is mainly controlled by the modifying the height and structure of tropopause (Fueglistaler & Haynes, 2005). Jain et al, (2010) reported that the extreme low cold point tropopause (CPT) temperatures ($\leq$ 191 K) are often observed during the monsoon season over the Bay of Bengal (BOB) and adjoining areas. Borsche et al. (2007) reported that the observational evidence of extremely cold tropopause temperatures about -100^{o}C, however, meteorological condition behind such extreme cold tropopause is not known completely.

On day-to-day scale, CPT height (H_{CPT}) and temperature (T_{CPT}) sometimes varies extremely which have been ignored due to its rare occurrence and due to complex UTLS processes. The complexity arises due to interlinked physical, chemical and dynamical processes. In this paper, we have attempted to examine the extreme variation of the CPT using regular radiosonde launches at 17:00 IST over Gadanki (13.5^{o}N, 79.2^{o}E) during 2006-2014. The

plausible roles of the convection, radiative heating due to water vapor and ozone, and equatorial wave propagation is explored to link the occurrence of the extreme tropopause. Data analysis and methodology are given in section 2. In section 3 results are presented and finally and discussion and conclusions are provided in section 4.

2 Database

2.1 GPS Radiosonde data

We have used high-resolution GPS radiosonde data observed regularly almost every day at ~1700 IST (IST = UT + 0530 h) during 18 April 2006 – November 2014 over Gadanki (13.5^{o}N, 79.2^{o}E), a tropical station, located at 375 m above mean sea level. In total 2487 radiosonde soundings are available with major data gaps during April – May 2007, March 2011, December 2012, January – February 2013 and April 2013 due to some technical reasons. Out of which 42 are rejected either due to balloon burst height below the tropopause and due to bad data quality. Remaining 2445 profiles of temperature are utilized to obtain the CPT temperature (T_{CPT}) and height (H_{CPT}). More details about radiosonde can be found in Mehta et al. (2010); (Mehta, Ratnam, & Murthy, 2011).

2.2 Infrared Brightness Temperature (TBB) data

To investigate the role of deep convection on the extreme variability of the tropopause we have used globally merged Infrared Brightness Temperature (TBB) observation obtained from national weather service Climate Prediction Centre, NOAA. This is Globally-merged, having the full-resolution up to ~4 km IR data formed from the ~11-micron IR channels aboard the GMS-5, GOES-8, Goes-10, Meteosat-7 and Meteosat-5 geostationary satellites. The TBB data is available with a time resolution of one hour and spatial resolution of 0.03˚ × 0.03˚ latitude – longitude. For our purpose, we have averaged the TBB data into 0.5˚× 0.5˚ (latitude-longitude)

centred to Gadanki and within ±1 and half hours of 1700 IST. The cloud top height (CTH) obtained as the altitude equivalent to TBB from the corresponding radiosonde temperature profiles for each extreme tropopause cases.

2.3 Microwave Limb Sounding (MLS) data

MLS of the Earth Observing System (EOS) on-board NASA's EOS Aura satellite is operational since August 2004. Aura-MLS provides high-resolution data from the ground to about 90 km. We have obtained the water vapor (H_2O) and ozone (O_3) profiles within 1-degree latitude-longitude around Gadanki using Microwave Limb Sounder (MLS) during 2006-2014. Water vapour profiles were retrieved from the radiance measurements of ~ 190 GHz rotational line and available between pressure levels 316 hPa to 0.02 hPa. The ozone profiles were retrieved from the radiance measurements of ~ 240 GHz and available between pressure levels 261 hPa to 0.02 hPa. In this study water and ozone profiles between the pressure level, 150-60 hPa is obtained on the days of extreme tropopause events.

3 Results

3.1 Identification of the extreme tropopause variability

Figure 1 shows the day-to-day variations of the T_{CPT} (Fig 1a) and H_{CPT} (Fig 1b) along with 30-point running mean over the period 2006–2014. Both T_{CPT} and H_{CPT} clearly shows annual cycles with colder and higher CPT during NH winter and warmer and lower CPT during NH summer. However, the annual cycle in H_{CPT} is better characterized when compared to T_{CPT} and hence their relationship is not exactly linear one (Mehta, Ratnam, & Murthy, 2011; Reid & Gage, 1996). The H_{CPT} and T_{CPT} are weakly anti-correlated (–0.30) significant at 95% confidence level. The correlation (–0.45) slightly improves by removing or smoothing high-frequency variabilities. It indicates that these high-frequency variabilities occur without preference of the

season. It is observed that T_{CPT} and H_{CPT} though represent the same parameter appears to be governed by different processes. Within the seasonal variations, CPT shows high-frequency variabilities which are mainly known to be due to day-to-day weather fluctuations (Mehta et al., 2010), planetary wave activities (Tsuda et al., 1994) and stratosphere-troposphere exchange processes. The interannual variations in CPT are mainly governed by the QBO and ENSO. However, in this study, we focus on the extreme variabilities within the seasonal variations.

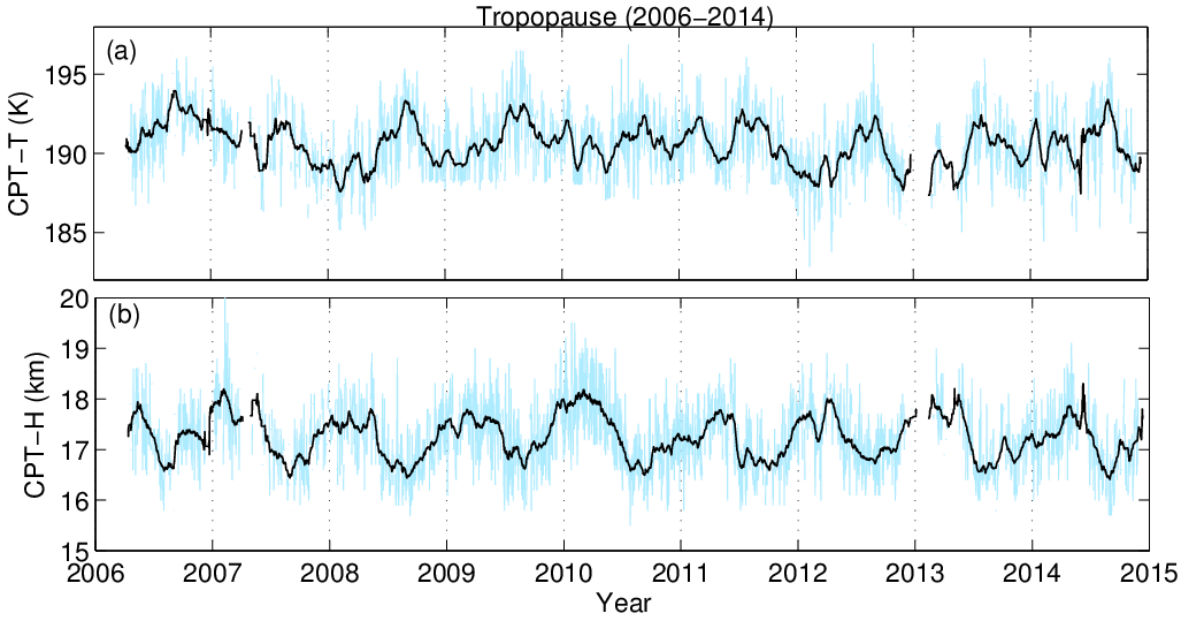

Figure 1. Timeseries of the daily variation of the (a) CPT–T and (b) CPT–H observed over Gadanki during 2006-2014. Heavy solid curve represents the 30–point running mean.

We obtained the climatological monthly mean, 1σ (standard deviation), 2σ and 3σ variations of the T_{CPT} and H_{CPT} for the years 2006−2014 as shown in Figure 2. On day-to day basis, CPT over Gadanki varies extremely. H_{CPT} is found to be as low as ~15.5 km and as high as ~19.5 km whereas T_{CPT} is cold as ~183 K and as warm as ~196 K several times. However, most of studies present climatology of the CPT as mean and ±1σ (Mehta et al., 2010; Seidel et al., 2001) which generally does not represent these extreme variations. We have obtained the probability distributions of the T_{CPT}, H_{CPT}, ΔT_{CPT} and ΔH_{CPT} where Δ represents the day-to-day

difference (tendency) as shown in Fig 3. It is interesting to note that these distributions are nearly Gaussian type. It is to be noted that, over the subtropics, the distribution of the tropopause height and temperature are bimodal with peaks at ~12 km and ~16 km due to the influence of the subtropical jet (STJ) (Pan et al., 2004) indicating the frequent occurrence of the multiple tropopauses. Whereas over Gadanki the normal distribution of the T_{CPT} and H_{CPT} indicate that the frequent occurrence of the sharp tropopause and less occurrence of the multiple tropopauses and broad tropopause.

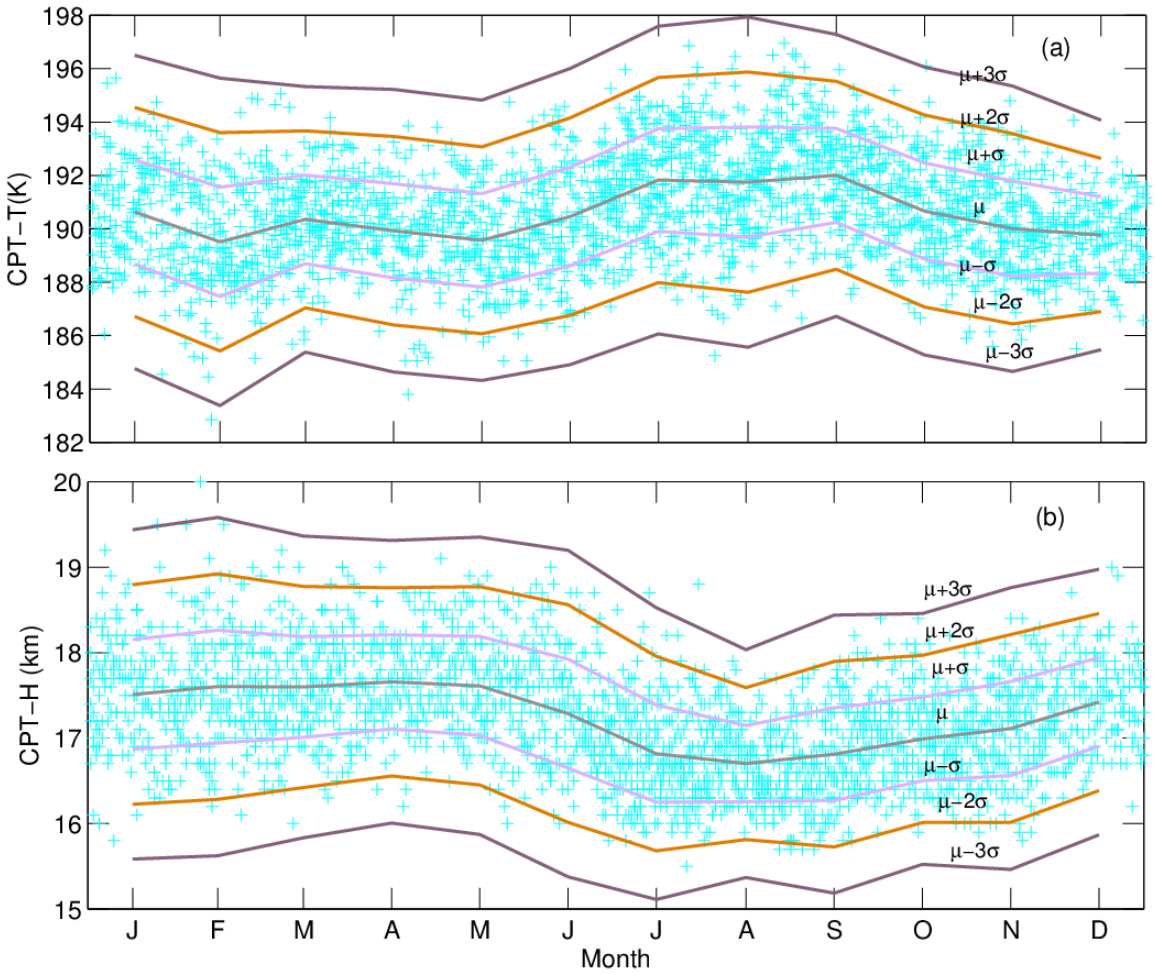

Figure 2. The daily variations of the (a) CPT–T and (b) CPT–H for each individual years between 2006–2014 along with their monthly mean (μ) and one, two and three standard deviations (σ) over the period 2006-2014.

As mentioned earlier, we have 2445 observations of the T_{CPT} and H_{CPT} over the period 2006–2014. Out of which about 67%, 95% and 99.7% of the variabilities fall within ±1σ, ±2σ and ±3σ respectively. There is a clear peak (mode) in the T_{CPT} (190.5 K) and H_{CPT} (17.3 km) which closely coincides with their mean T_{CPT} and H_{CPT}, respectively (see Table 1). Thus, 67% of the T_{CPT} and H_{CPT} ranges from 188.6 K to 192.6 K and 16.6 km to 17.9 km, respectively. About 28% of the T_{CPT} ranges ~185.4–190.2 K and ~191.6–195.9 K while H_{CPT} ranges ~15.7–17.1 km and ~17.1 – 18.9 km. Remaining 5% varies extremely with T_{CPT} < 188.5 K, T_{CPT} > 195.9 K, H_{CPT} < 16.5 km and H_{CPT} >17.6 km, we termed them as the coldest, warmest, lowest and highest tropopause, respectively. Over Gadanki, the distribution of the ΔT_{CPT} reveals that T_{CPT} fluctuates within ±2 K for ~67% cases, between ±2 K and ±4 K for ~28% cases and greater (less) than 4 K (–4K) for ~ 5% cases on day-to-day basis (Fig 3c). Similarly, the distribution of ΔH_{CPT} reveals that H_{CPT} fluctuates within ~ ±0.7 km for ~ 67% cases, between ±0.7 km and ±1.4 km for ~28% cases and greater (less) than 1.4 km (–1.4 km) for ~ 5% cases on a day to basis (Fig 3d). Thus, those cases when H_{CPT} (T_{CPT}) increases or decreases by 1.4 km (4 K) are regards as extreme cases. In other words, those T_{CPT} and H_{CPT} which vary more than the values 2σ form their climatological monthly mean are termed as extreme cases. That is the extreme variability in the T_{CPT} and H_{CPT} are identified based on the 2σ departure from their climatological monthly mean. Climatological monthly mean T_{CPT} and H_{CPT} are represented as μT_{CPT} and μH_{CPT}, respectively and their standard deviations as σT_{CPT} and σH_{CPT}, respectively. Thus, coldest (warmest) tropopause is defined as T_{CPT} is lesser (greater) than $\mu T_{CPT} - 2\sigma T_{CPT}$ ($\mu T_{CPT} + 2\sigma T_{CPT}$). Similarly, the highest (lowest) tropopause is defined as H_{CPT} is greater (lesser) than $\mu H_{CPT} - 2\sigma H_{CPT}$ ($\mu H_{CPT} - 2\sigma H_{CPT}$).

3.2 Temporal distributions and occurrence of the extreme tropopauses

In total 161 extreme cases of the CPT are found over the period 2006-2014 which are used for further analysis. Out of which 52, 30, 57, and 22 cases are found as the coldest, warmest, highest and lowest tropopauses, respectively. To understand the behavior of the temperature structure neighborhood to the extreme tropopauses, we have juxtaposed the temporal occurrences of the extreme tropopauses over the time-height section of the temperature anomalies between altitudes 14-20 km for the period 2006-2014 are shown in **Figure 4**. For clarity, we have also plotted the temporal distribution of the extreme H_{CPT} and T_{CPT} separately as shown in the Supplementary Figures S1 and S2. It is clear that the coldest and highest tropopauses are distributed throughout the season and not preferably in the northern hemisphere (NH) winter (DJF) season. Similarly, the warmest and lowest tropopauses occur randomly in all the seasons and not preferably in the NH summer (JJA) season. It is also evident that the coldest and highest tropopauses occur independently. That is the coldest tropopause are not the highest one and vice versa. Similarly, the warmest and lowest tropopauses also occur independently except for 4 cases.

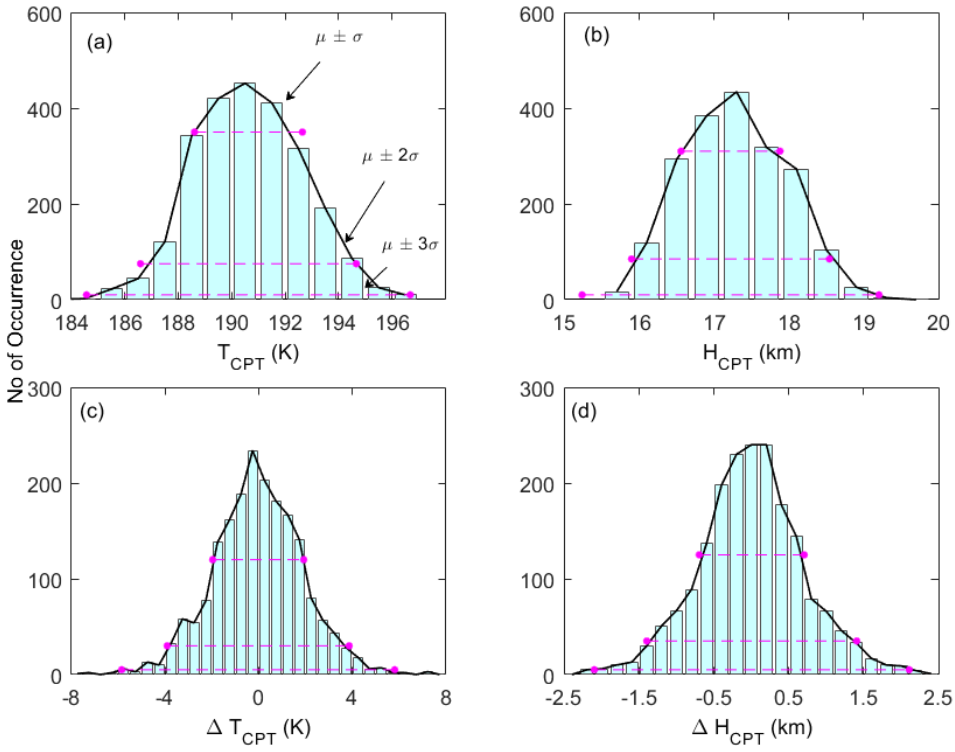

Figure 3. Probability distribution of the daily values of the (a) T_{CPT}, (b) H_{CPT}, (c) ΔT_{CPT} and (d) ΔH_{CPT} along with μ ± σ, μ ± 2σ and μ ± 3σ lines indicated as horizontal dashed lines observed over Gadanki during 2006-2014. ΔT_{CPT} and ΔH_{CPT} represents the daily difference.

The number of occurrences of the coldest, warmest, highest and lowest tropopauses, their mean and standard deviation during different seasons is shown in **Figure 5**. Overall, the occurrence of extreme cases is minimum during NH winter and maximum during NH summer season. It indicates that the extreme cases occur throughout the year and without any preference to season. It is interesting to note that the coldest tropopause occurs more frequently during NH summer season and not in NH winter season. It supports the earlier finding that coldest tropopause occurs more frequently during NH spring and summer season over the Indian monsoon region (Jain et al., 2006; Newell & Gould-Stewart, 1981). The lowest tropopause occurs more frequently during NH winter season when compared to NH summer season.

233 However, though tropopause is higher and colder during NH winter, highest tropopause
234 frequently occurs during NH summer. During summer monsoon season deep convection
235 frequently occurs over this location which could be a possible reason for the frequent occurrence
236 of the highest tropopause during this season. However, as tropopause is lower and warmer
237 during NH summer season, the warmest tropopause also occurs more frequently during this
238 season.

239 The seasonal mean of the coldest tropopause T_{CPT} varies from 185.1±1.1 K (in DJF) to
240 187.1±0.7 K (in JJA) and their corresponding H_{CPT} from 17.0±0.25 km (in JJA) to 17.5±0.53 km
241 (in DJF). The coldest tropopause T_{CPT} shows a similar seasonal structure as the climatological
242 mean T_{CPT} (190-192K). However, the T_{CPT} of the coldest case is always colder by about 4-5 K
243 from the climatological mean tropopause T_{CPT} throughout the season. The H_{CPT} for the coldest
244 case also shows a similar seasonal structure as the overall monthly mean (16.8-17.5 km).
245 However, H_{CPT} of the coldest case occurs at the same altitude of the climatological mean H_{CPT}.
246 Thus, it indicates that the coldest tropopause needs not necessarily represent the highest
247 tropopause.

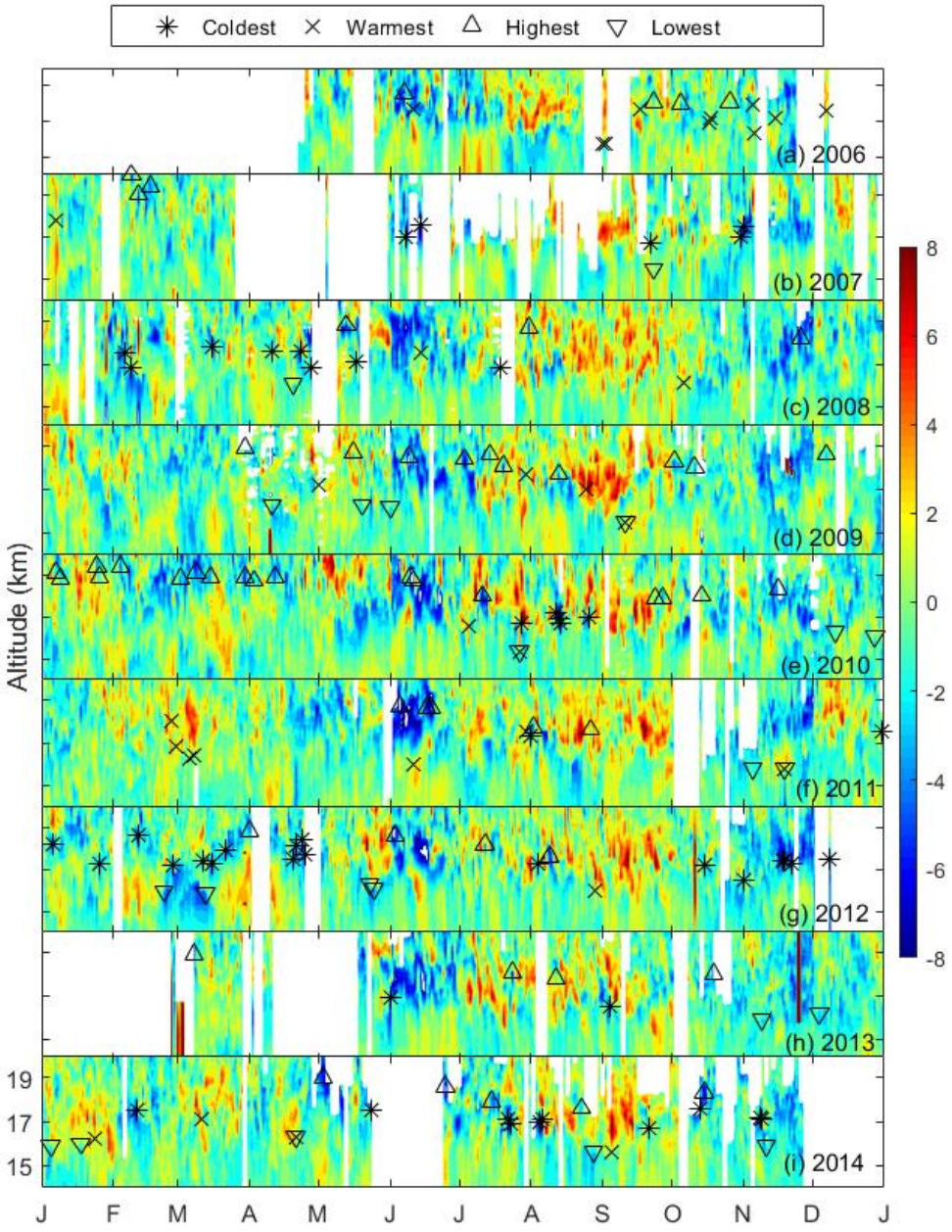

Figure 4. (a)-(i) Time height sections of the temperature perturbation between 14 km and 20 km embedded with the extreme (Coldest, Warmest, Highest, Lowest) CPT altitude for the period 2006-2014, respectively

The scatter plot between coldest T_{CPT} and their corresponding H_{CPT} (**Figure 6a**) shows that there are only three cases of the coldest tropopause which occur above 18 km. Among them, the extremely coldest tropopause (T_{CPT} =182.8 K, H_{CPT} =18.6 km) occurred on 11 February 2012 (Supplementary Figure S3a). The majority of the coldest tropopauses are ranging between 16.5

km to 17.5 km. It can be seen that the coldest tropopause even occurs as low as at ~ 16.5 km which has T_{CPT} < 188 K. The T_{CPT} for the coldest cases is always colder than 191 K suggesting entry of drier air into the stratosphere over Gandaki. About half of the total observations T_{CPT} remains colder than ~ 191 K indicating that the entry of water vapor into the stratosphere with mixing ratio less than 3.0 ppmv (Figure 3). The T_{CPT} and corresponding H_{CPT} for the coldest tropopause are moderately anticorrelated (r = -0.53) significant at 95% confidence level (Fig. 6a).

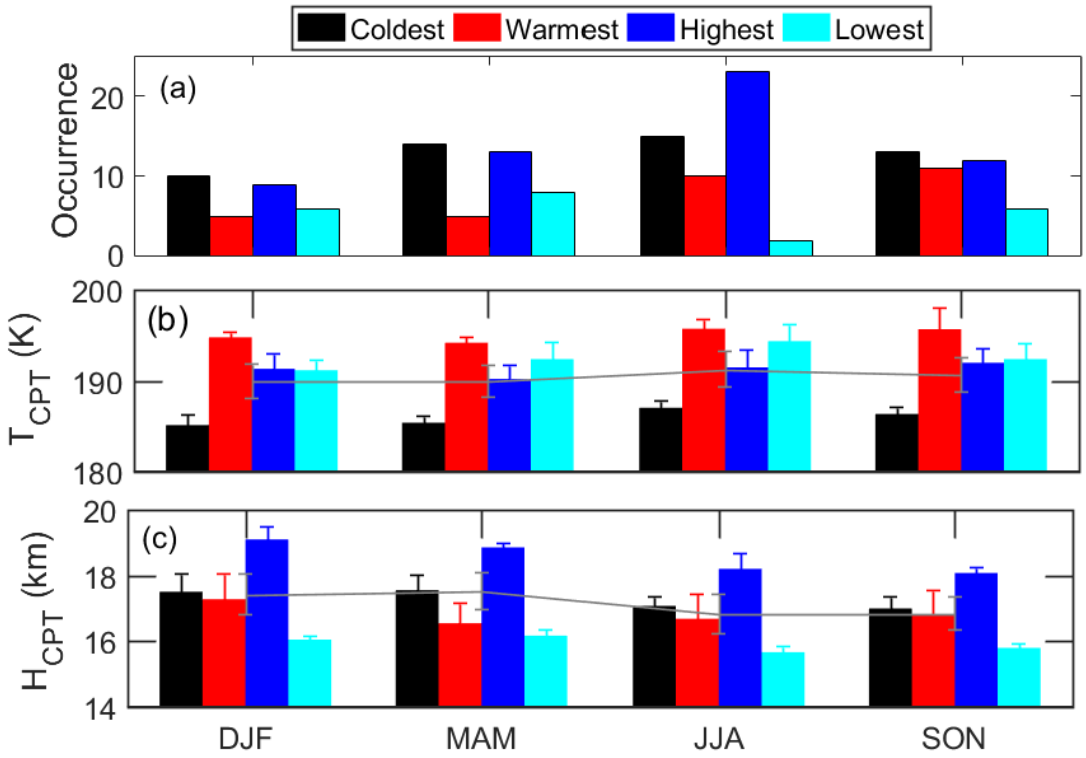

Figure 5. Season-wise (a) occurrence of CPT (b) mean and SD of the CPT-T and (c) mean and SD of the CPT-H for the coldest, warmest, higest and lowest cases observed during 2006-2014.

Similarly, the seasonal mean T_{CPT} for the warmest case varies from 194.4±0.54 K (in MAM) to 196.1±0.9 K (in JJA) and their corresponding H_{CPT} varies between 16.7 ±0.45 km (in MAM) to 17.3±0.76 km (in DJF) throughout the year. The T_{CPT} for the warmest case is warmer by 4-5 K from the climatological mean tropopause. The scatter plot between T_{CPT} and their corresponding H_{CPT} (Figure 6b) shows that the warmest tropopauses are seen to occur at about ~

18 km several times. It indicates that these warmest tropopauses though occurring at higher heights need not be necessarily the coldest tropopause. The typical warmest tropopause (H_{CPT} =16.2 km, T_{CPT} =194.8 K) is observed on 23 January 2014. In general, the warmest tropopause T_{CPT} and H_{CPT} show insignificant anti-correlation (r = -0.37).

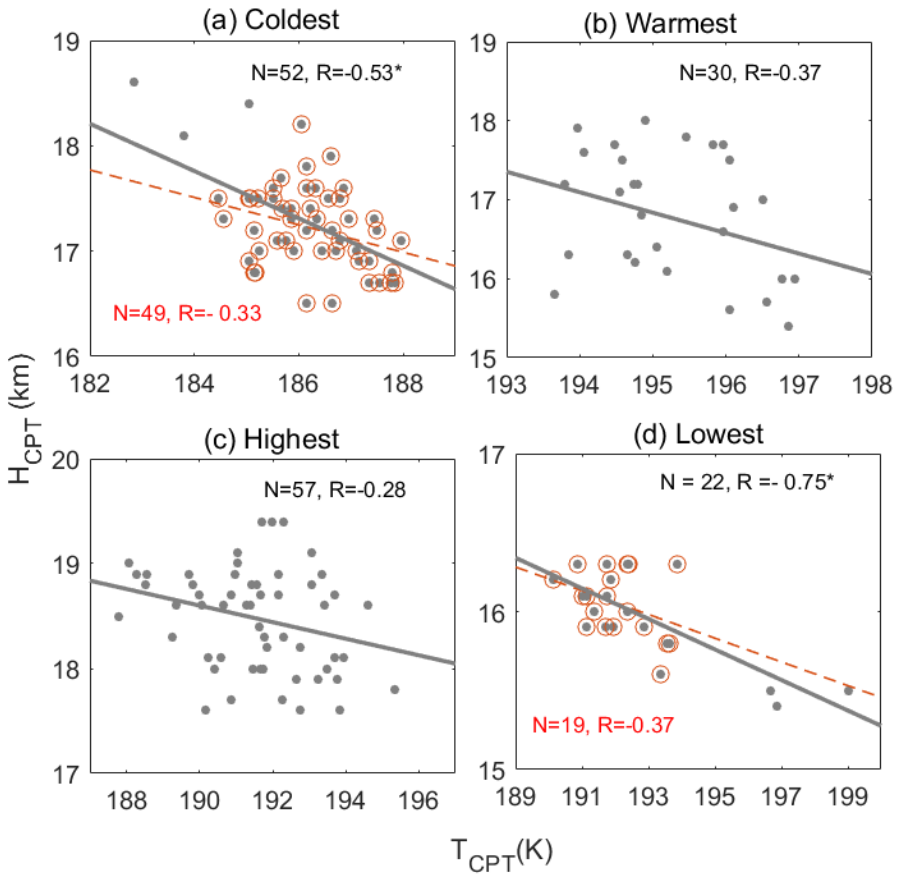

Figure 6. Scatter plot between CPT-H and CPT-T for the (a) coldest, (b) warmest, (c) highest and (d) lowest cases.

The seasonal mean H_{CPT} for the highest tropopause ranges from 18.1±0.15 km (SON) and 19.17±0.4 km (DJF) and their corresponding mean T_{CPT} varies between 190.6±1.5 K (in MAM) to 192.3±1.3 K (in SON). The H_{CPT} for the highest case is higher by ~ 1.0 - 1.7 km from the climatological mean tropopause. From the scatter plot, it can be seen that only a few highest tropopauses are colder than 191 K. The typical highest tropopause (H_{CPT} =19.4 km, T_{CPT} =192.3 K) is observed on 02 February 2007. Similar to the warmest tropopause, T_{CPT} and H_{CPT} for the

highest tropopause case are insignificantly correlated (r = -0.28). In this case, T_{CPT} has poor seasonal structure when compared to H_{CPT}.

The seasonal mean H_{CPT} for the lowest tropopause ranges from 15.5±0.14 km (JJA) and 16.19±0.14 km (MAM) and their corresponding mean T_{CPT} varies between 191.7±0.83 K (in DJF) to 195.1±2.5 K (in JJA). The H_{CPT} for the lowest case is lower by ~ 1.0 - 1.3 km from the climatological mean tropopause. Even though lowest tropopauses are occurring at a lower altitude, there are several cases when they attain temperature less than 191 K. One such typical (most) lowest tropopause (H_{CPT} =15.4 km, T_{CPT} =196.9 K) is observed on 26 July 2010 (Supplementary Fig S3d). This typical temperature profile also shows the secondary tropopause (H_{CPT} =17.4 km, T_{CPT} =197 K) ~2 km above the coldest tropopause. Over Gadanki, in general, we have observed that the lowest tropopauses are associated with double tropopause (Mehta et al., 2011).

Thus, the temporal distributions of the extreme tropopauses reveal that they occur independently except a few. That is the coldest CPT needs not to be the highest CPT and vice versa and the warmest CPT needs not to be the lowest CPT and vice-versa. The correlation between T_{CPT} and H_{CPT} of the extreme tropopauses shows negative correlation indicating that they broadly agree with ‘higher and colder’ and ‘lower and warmer’ tropopause characteristics, however, not always. The overall monthly variation of the coldest and lowest tropopause shows higher and colder during NH winter and lower and warmer during NH summer season (Supplementary Figure S4) resulting into T_{CPT} and H_{CPT} are anti-correlated. Whereas for the warmest and highest tropopause T_{CPT} and H_{CPT} are not significantly anti-correlated. For the warmest case, T_{CPT} becomes colder and warmer during NH winter and summer, respectively, but not the H_{CPT} which shows uniform variation throughout the year (Supplementary Figure S4).

Similarly, for the highest tropopause case, H_{CPT} is higher during NH winter and lower during NH summer seasons but T_{CPT} has very poor seasonal variation and appears roughly uniform throughout the year (Supplementary Figure S4).

Mehta et al., (2011) have investigated the minimum and maximum CPT altitudes calculated for each grid box using COSMIC GPS RO data, and their global distribution (within ±30° latitude) during different seasons. They observed that the CPT altitude has a large variation ranging from 15 km to 19 km. The minimum CPT altitude ranges from 15-16.4 km and maximum CPT altitude ranges from 17-18.6 km. These minimum and maximum CPT altitudes are similar to the lowest and highest tropopause, respectively.

3.3 Mean thermal structure of the extreme tropopause

We have segregated all the temperature profiles between 12 and 22 km for the coldest, warmest, highest and lowest cases and obtained their mean profiles as shown in **Figure 7**. The mean temperature of these extreme cases reveals that their thermal structures are distinct. It is interesting to note that individual extreme temperature profiles under different extreme cases possess similar thermal structures. For the coldest cases, the tropopauses are sharper while the rest of other cases is border. Again, these broader cases are different among themselves. For the warmest tropopause cases, the temperature between ~16 km to 18.5 km is nearly constant ($\frac{dT}{dz} \cong 0$). For the highest tropopause cases, the temperature between ~ 16 km to 18.5 km slightly decreases ($\frac{dT}{dz} < 0$). For the lowest tropopause cases, the temperature increases ($\frac{dT}{dz} > 0$) slowly (i.e., having very small lapse rate) with an altitude between ~ 16 km to 18.5 km. Figure 5e shows the comparison of the mean thermal structure of these extreme cases which reveals a tropopause region bounded by the lowest mean tropopauses at ~ 16 km as lower boundary and highest mean tropopause at ~ 18.5 km as the upper boundary. It is the region within which thermal structure is

mostly perturbed in a well-defined way whose occurrence results into large day to day variation in the tropopause. About one km below and above this tropopause region, all these extreme tropopause temperature profiles represent about the same mean structure.

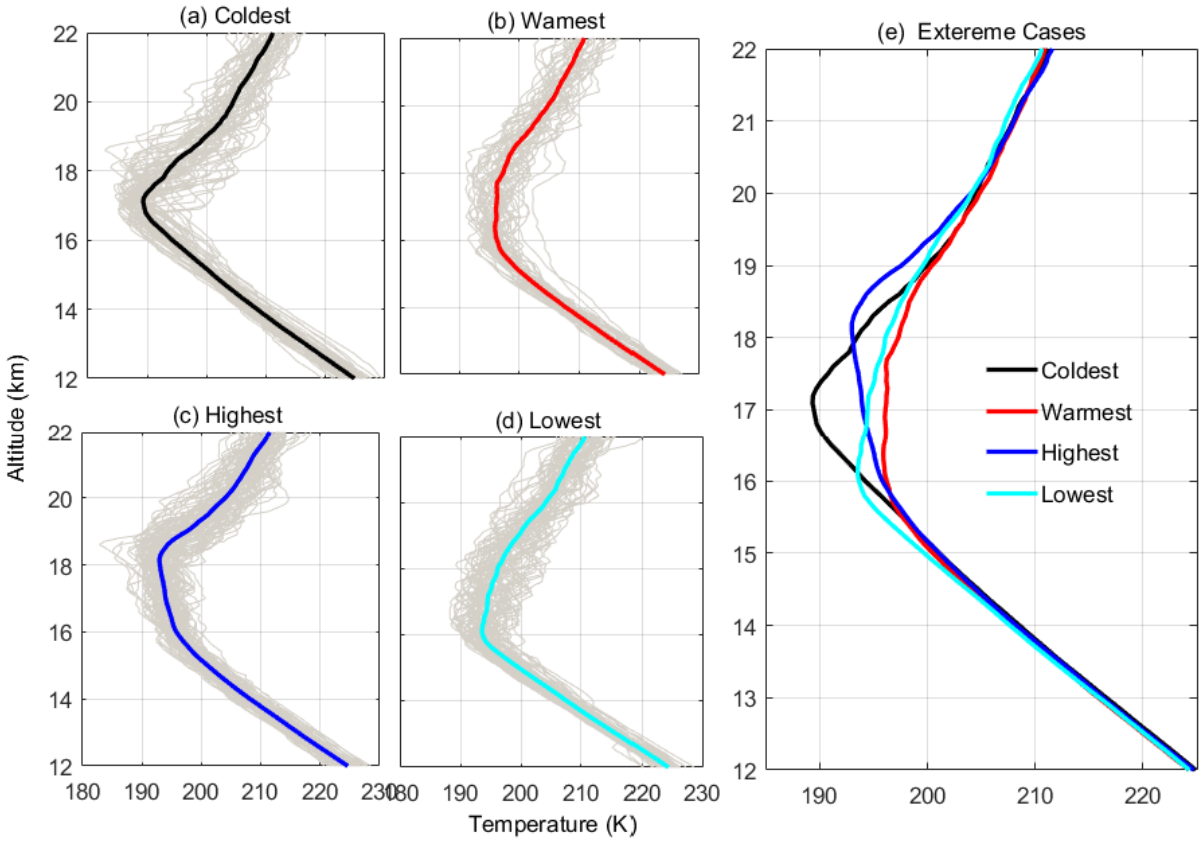

Figure 7. All individual and their mean temperature profiles observed for the (a) coldest, (b) warmest, (c) highest, and (d) lowest. (e) Represents the thermal structure for different extreme cases.

Supplementary Figure S5 presents the mean and SD of the temperature, height and sharpness for the coldest, warmest, highest and lowest tropopause cases. As mentioned earlier, the coldest tropopause means temperature is ~186.1±1.1 K much colder than the threshold temperature (191 K) required for the freeze-drying of air enters into the lower stratosphere. Such coldest tropopause would result in the extreme dryness of the lower stratosphere as originally explained by Dobson et al. (1946) and Brewer (1949). The coldest tropopauses height

345 (17.30±0.47 km) occurs nearly at the same height where NH winter tropopause (17.5±0.5 km) is
346 commonly formed. These coldest tropopauses are generally sharper (7.83±1.73 $\times 10^{-4} s^{-2}$).

347 **3.4 Ozone and water vapor Variability during extreme days**

348 In a case study, Takashima et al. (2010) observed extremely low temperatures near the
349 tropical tropopause associated with the minimum water vapor and higher frequency of cirrus
350 clouds occurrence. The annual minimum for tropopause height in July and August is
351 accompanied by the warmest tropopause temperatures, which implies higher saturation mixing
352 ratios for water vapor and higher temperature thresholds for the formation of ice particles for this
353 season. To understand the role of the ozone and water vapor on the extreme tropopauses, we
354 have collected the MLS data closest to the Gadanki for the extreme days during 2006-2014. In
355 total 26 ozone and water vapor profiles are found on the extreme tropopause cases.

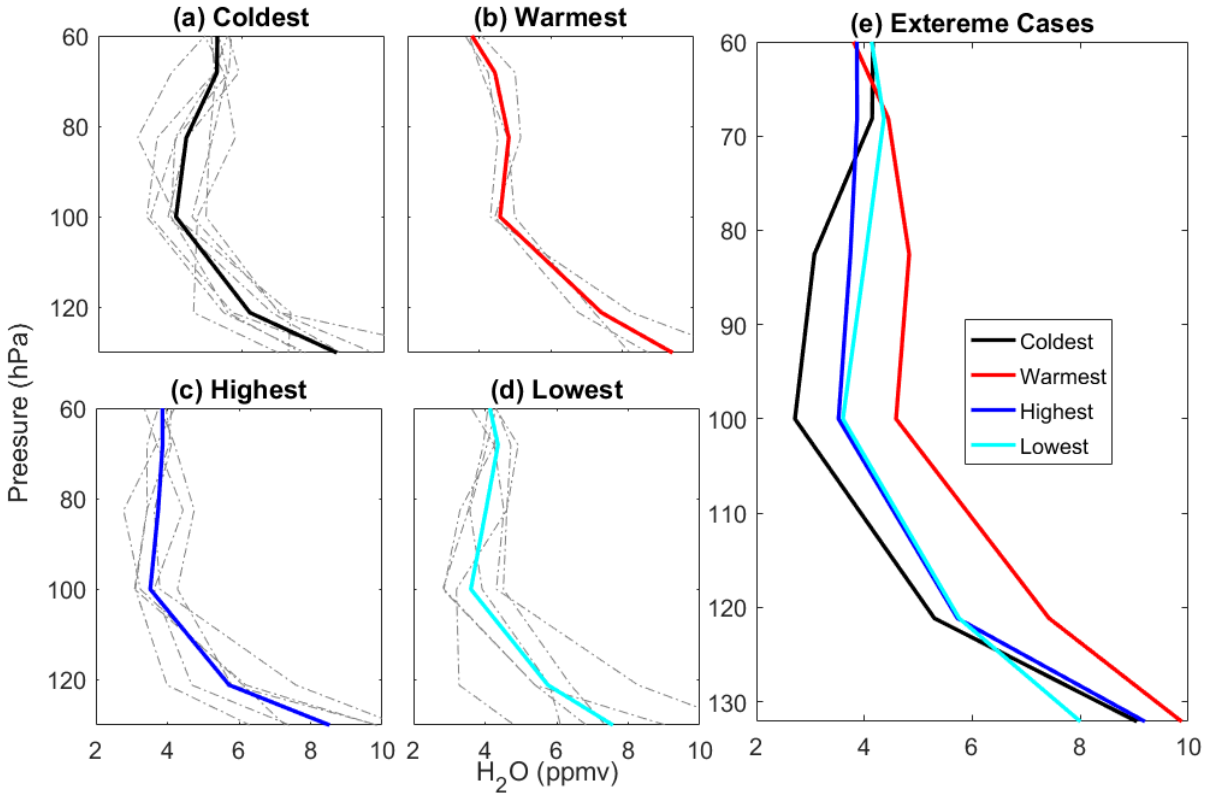

356
357 Figure 8 same as Figure 7 but observed water vapor profiles. Vertical coordination in hPa.

358

359 **Figure 8** shows all the water vapor profiles and their corresponding means between
360 pressure levels 130 hPa to 60 hPa for the coldest, warmest, highest and lowest tropopause cases.
361 It is interesting to note that the vertical structures of the water vapor for each individual extreme
362 tropopause cases are similar. These extreme cases though similar have the similar vertical
363 structure they show large variability. The water vapor is found to be minimum between 120-80
364 hPa for the coldest tropopause cases and maximum for the warmest tropopause cases. The water
365 vapor at 100 hPa is 2.7, 4.6, 3.5, and 3.6 ppmv for the coldest, warmest, highest and lowest
366 tropopause cases, respectively.

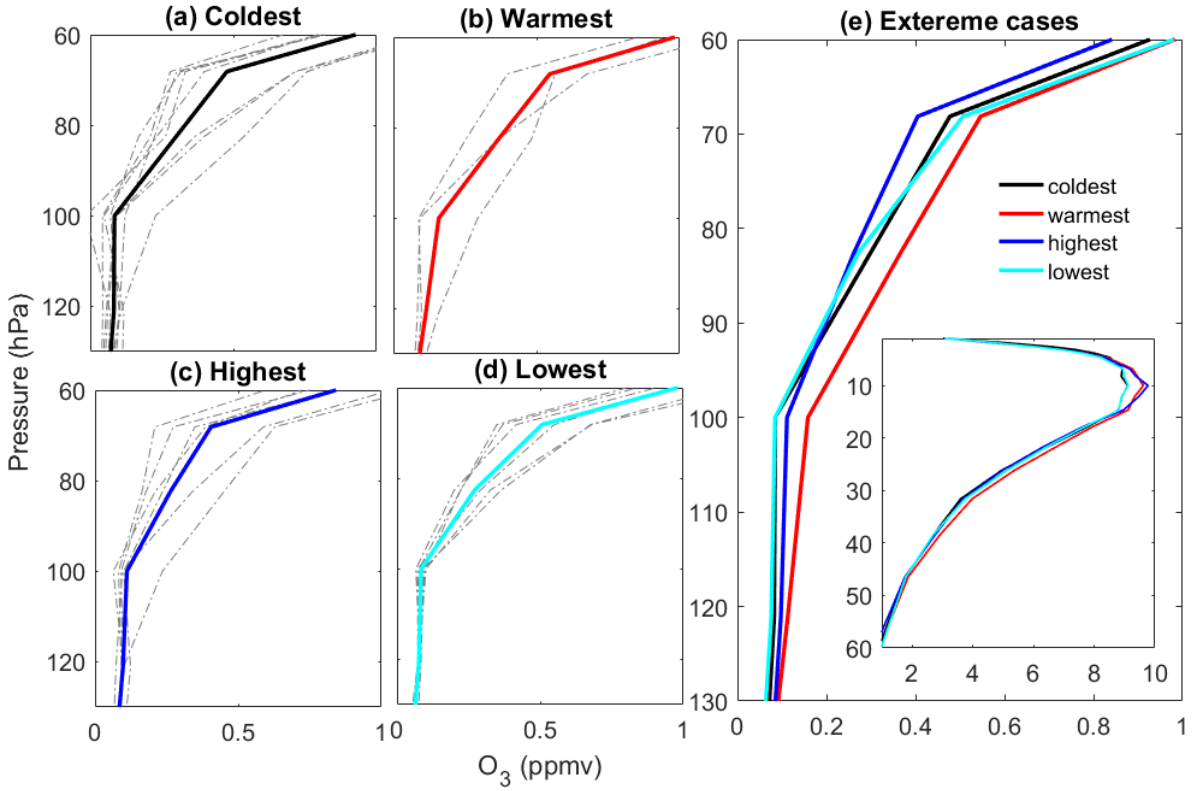

367
368 Figure 9 Same as Figure 7 but observed for ozone profile. Vertical coordination in hPa.
369

370 **Figure 9** shows all the ozone profiles and their corresponding mean between 130 hPa and
371 60 hPa for the coldest, warmest, highest and lowest tropopauses. Although we have a very

limited number of ozone observations, the distinct structure of ozone profiles suggests that ozone plays a significant role in the occurrence of extreme tropopause and its day-to-day variability. It is well known that the ozone absorbs UV radiation and radiatively warm the stratosphere. As expected, for the warmest tropopause cases ozone concentrations are found to be more when compared to the coldest tropopause. It means that the warmest tropopause occurs with high ozone concentrations in the lower stratosphere while the coldest tropopause occurs with low ozone concentrations in the lower stratosphere. The inset picture shows the variability of the ozone peak with extreme tropopause cases. It is interesting to observe the higher ozone concentrations for the warmest and highest tropopauses when compared coldest and lowest tropopauses. The possible link between extreme tropopauses and ozone peak variability cannot fully be ascertained with this limited dataset and needs to be investigated in details.

3.5 Role of convection

It is well known that the convection plays an important role in the modification of the tropical tropopause structure (Muhsin et al., 2018; Sherwood et al., 2003). Muhsin et al. (2018) have examined the role of the different types of the convection on the variation of the tropical tropopause parameters over Gandaki and reported that H_{CPT} lowers with the increase in convective strength from shallow to deep convection. We have performed the similar analysis to examine the role of convection on the occurrence of the extreme tropopauses using the IRBT data over the period 2006-2014 following Meenu et al. (2010) and segregated all the extreme tropopauses and the corresponding temperature profiles based on the different types of the convective clouds occurring at different altitudes. For the clear sky, IRBT>280K corresponds to cloud top altitude (H_{CCT})< 2 km. For convective clouds (H_{CCT} > 2km), the IRBT thresholds are considered as (i) 280 – 270 K corresponding to H_{CCT} = 2 – 5 km, (ii) 270 – 245 K corresponding

395 to H_{CCT} = 5 – 8 km (iii) 245– 235 K corresponding to H_{CCT} = 8 – 10 km, (iv) 235 – 220 K
396 corresponding to H_{CCT} = 10 – 12 km, and (v) <220 K corresponding to H_{CCT} > 12 km.

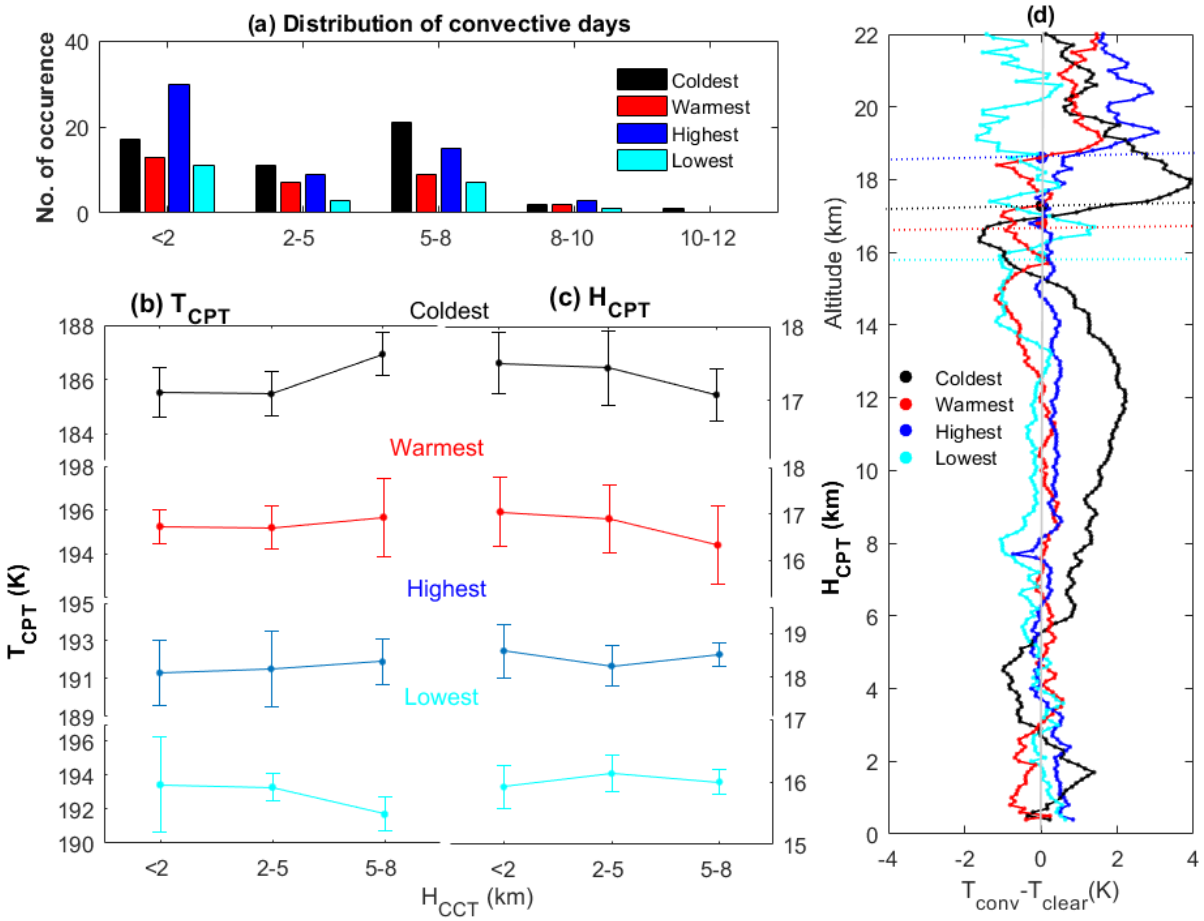

397
398 **Figure 10. (a)** Distribution of the occurrence of the extreme tropopauses for the clear sky (<2 km) and convective
399 clouds with top between 2 and 5 km, 5 and 8 km, 8 and 10 km and 10-12 km. (b-c) The mean and one standard
400 deviation of the T_{CPT} and H_{CPT} for the extreme tropopause under the clear sky, convective clouds with top between 2
401 and 5 km and 5 and 8 km. (d) Vertical profiles of temperature anomaly (subtracted by clear sky temperature
402 profiles) of convective top between 5 and 8 km. Horizontal dashed lines indicates the H_{CPT} for the respective
403 extreme tropopauses.
404

405 **Figure 10a** shows the distributions of the clear sky and convective days for the extreme
406 tropopause cases. Out of 161 extreme cases, 71 days are falling under clear sky days while 90
407 cases for the convective days. Out of 90 convective days, 30, 51, 8 and 1 days are observed for
408 H_{CCT} = 2 – 5 km, 5 – 8 km, 8 – 10 km and 10 –12 km, respectively. **Figures 10 b-c** shows the
409 mean and standard deviation of the T_{CPT} and H_{CPT} for the clear sky (H_{CCT} < 2 km), H_{CCT} = 2 – 5

km, and H_{CCT} =5 – 8 km cases. Other convective cases are not shown due to the inadequate number of observations. Out of 30 (51) H_{CCT} = 2 – 5 km (H_{CCT} = 5 – 8 km) cases, 11 (21), 7(9), 9(15), and 3(7) are observed for the coldest, warmest, highest and lowest tropopauses, respectively. Under very shallow convective clouds (H_{CCT} = 2 – 5 km), extreme T_{CPT} do not show any significant change relative to clear sky condition. However, H_{CPT} for the coldest, warmest and highest tropopauses lower relative to clear sky condition. For the lowest tropopause, H_{CPT} becomes higher relative to clear sky condition. For the shallow convective clouds (H_{CCT} = 5 – 8 km), coldest tropopause becomes warmer by ~ 1.5 K and lower by ~0.5 km relative to clear sky condition. While the T_{CPT} remains unchanged and H_{CPT} lowers by 0.7 km for the warmest case, both T_{CPT} and H_{CPT} remain unchanged for the highest cases, and T_{CPT} becomes colder by ~ 1.7 K and H_{CPT} remain unchanged for the lowest case relative to clear sky condition.

Figure 10d shows the difference between the shallow convective temperature profiles and the clear sky temperature profile. We observed prominent warming of ~ 2 K between 8-14 km above the cloud top, cooling ~ 2 K just below the CPT (in the tropical tropopause layer) and warming ~ 4K at ~ 18 km just above the CPT in the lower stratosphere for the coldest tropopause case. Similar nature is also observed for the warmest and highest tropopauses cases however with smaller magnitudes. The anomalous warming above the cloud top is known due to the latent heat release from convective clouds (Houze Jr, 2004) as a direct response of convection while anomalous cooling (warming) just below (above) CPT could be an indirect response to convection (Gettelman & Birner, 2007; Johnson & Kriete, 1982; Muhsin et al., 2018; Paulik & Birner, 2012; Randel et al., 2003). The extreme tropopause temperature profiles show cooling below the CPT i.e in the tropical tropopause layer region (H. Kim & Dessler, 2004) which could

be either due to convective detrainment and turbulent mixing (Sherwood et al., 2003) or due to radiative cooling caused by reduction of longwave radiation (Webster & Stephens, 1980).

3.6 Role of equatorial wave in the extreme variability

Equatorial wave propagations in the tropopause region significantly modulate the tropical tropopause structure (Boehm & Verlinde, 2000; Munchak & Pan, 2014; Tsuda et al., 1994). These waves can modulate the $\mathbf{T_{CPT}}$ up to 8 K and $\mathbf{H_{CPT}}$ up to its vertical wavelength ~ 4 km (Boehm & Verlinde, 2000) which tropopause cause the tropopause to vary extremely. Several times extreme tropopause is associated with warm and cold temperature anomalies as mentioned in Fig 4. The role of the equatorial wave on the extreme variation of the tropopause is demonstrated by taking one such event of temperature anomalies associated with occurrence the coldest and lowest CPT observed during January- March 2012 as shown in **Figure 11**.

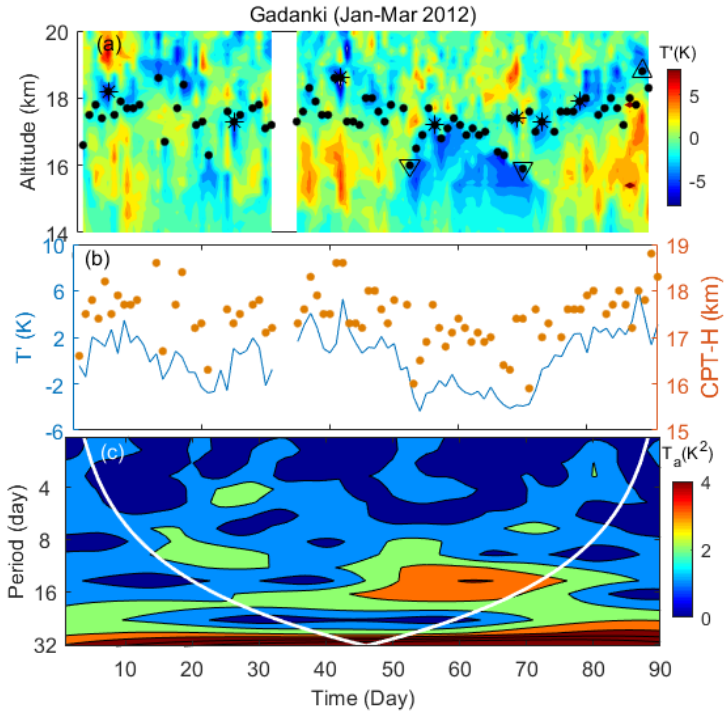

Figure 11. (a) Time height section of the contour plot of the temperature anomalies during January to March 2012 superimposed with H_{CPT}. (b) Time series of temperature anomalies averaged between 16 km and 17 km and H_{CPT}. (c) wavelet spectrum of temperature (in terms of power) at 16-17 km during January to March 2012. White curve in (c) represents the cone of influence.

448

449 During this period the H_{CPT} shows sinusoidal pattern indicating the wave propagation. There are
450 seven coldest tropopause cases occurred during this period. Among them, extremely coldest
451 tropopause with T_{CPT} ~182.8 K and H_{CPT} ~ 18.6 km is observed on 11 February 2012(See
452 Supplement Fig S3a). It is known that Kelvin wave amplitudes maximize near the tropopause
453 which sometimes modifies the tropopause structure significantly with the coldest tropopause
454 (Ratnam et al., 2006). The downward shift in the temperature anomalies and H_{CPT} can be clearly
455 noticed particularly on 2nd week of February to March 2012 indicating the influence of
456 downward phase propagating waves. In order to examine the role of equatorial planetary-scale
457 waves, the time series of temperature averaged between 16 km and 17 km is subjected to spectral
458 analyses (Morlet wavelet) to obtain the dominant wave periods and the times of their
459 occurrences. For this analysis, we have subtracted the January- March months mean temperature
460 profile from individual temperature profiles to obtain the fluctuation component which is
461 subjected to wavelet analysis. It is seen that waves with periods 10-20 days are significant from
462 15 February to 10 March 2012. The dominant periods within the cone of influence are only
463 considered in order to avoid edge effects. To ascertain the nature of these waves, the amplitude
464 and phase of the dominant wave periods in temperature and zonal wind during January-March
465 2012 for a 10-day period. It is observed that the amplitudes in temperature and zonal wind in the
466 altitude range 15-20 km are ~1.0 K and 2-3 m/s, respectively (Figure is not shown). The phase
467 shows clear downward propagation (upward propagating wave) with temperature phase leading
468 the zonal wind phase indicating the Kelvin wave propagation (Mehta et al., 2013). Since Kelvin
469 wave amplitudes are seen maximum near the tropopause, hence they can sometimes modify the

tropopause structure significantly with the coldest tropopause. Such coldest tropopause may occur due to the vertically propagating Kelvin wave (Tsuda et al., 1994).

4 Discussion and Conclusions

The regular observations of high-resolution GPS radiosonde launching over a tropical location, Gadanki, in the Indian monsoon region is used here to demonstrate the extreme variability of the tropical tropopause. Within the seasonal variations, CPT shows high-frequency variabilities which are mainly known to be due to day-to-day weather fluctuations, planetary wave activities and stratosphere-troposphere exchange processes(Holton et al., 1995; Mehta et al., 2010; Tsuda et al., 1994). The one sigma variation of the T_{CPT} (H_{CPT}) is ~ 2.0 K (0.66 km) over Gadanki, however, T_{CPT} (H_{CPT}) becomes extremely cold or warm (high or low) by ~4 K (1.32 km) from its mean temperature ~190.6 K (height ~ 17.21 km) for the significant number of times. The long-term observations of the radiosonde data provided us with an opportunity to collect the sufficient number of extreme tropopause cases identified as the cases falling outside the two-sigma level of climatological mean tropopause over the period 2006-2014. Over Gadanki, the probability distribution of the T_{CPT} and H_{CPT} is nearly Gaussian. The coldest (warmest) tropopause is defined if T_{CPT} is lesser (greater) than the lower (upper) limit of its two-sigma level whereas the highest (lowest) tropopause is defined as the H_{CPT} is greater (lesser) than the lower (upper) limit of its two-sigma level. The extreme tropopause cases are found to be about 5% (161) of the total data over the period 2006-2014. Out of which 52, 30, 57, and 22 cases are found as the coldest, warmest, highest and lowest tropopauses, respectively. Though these cases of the tropopause play a significant role in the tropopause variability they considered as rare or outliers and remain ignored.

Based on the seasonal variation, the tropopause is defined as the colder and higher tropopause during NH winter and warmer and lower tropopause during NH summer (Seidel et al., 2001). However, our finding here demonstrates that the coldest and highest (warmest and lowest) tropopauses occur throughout the year and not only during NH winter (summer) season. The occurrence of the coldest and highest tropopause is more frequent during NH summer and not during the NH winter due to frequent occurrence of the deep convection during the former season (Newell & Gould-Stewart, 1981). These extreme cases occur independently; that is coldest (warmest) one need not be necessarily the highest (lowest) and vice versa. Our observation shows that these extreme tropopause cases have a unique vertical structure. The distinct thermal structures of the mean temperature profiles of these extreme cases reveal that the coldest tropopause is sharper while warmest, highest and lowest tropopauses are border characterized as unique lapse rate between ~16 km to 18.5 km which are nearly equal to zero, greater than zero and lesser than zero, respectively.

The possible mechanisms for the occurrence of the extreme tropopause cases such as deep convection, propagation of the equatorial wave, stratosphere-troposphere exchange processes and the occurrence of the cirrus clouds. Extreme variations in the tropopause altitude may have a direct bearing on the energy source for the stratospheric motions, the exchange of water vapor and ozone between troposphere and stratosphere (Holton, 1982). Our observation of high abundance of the water vapor and ozone concentrations for the warmest tropopause and low water vapor and ozone concentrations for the coldest tropopause indicating its possible role in modulating the thermal structure of the tropopause radiatively. However, the role radiative effects on the temperature and the tropopause variation due to water vapor and ozone are not easy to quantify as they are associated with the deep convection events. It is well known that the

515 transport of the tropospheric water vapor into the UTLS, as well as the intrusion of the ozone
516 rich air to upper troposphere, are mainly associated with deep convection events.

517 The role of the convection on the tropical tropopause is well known and it is found H_{CPT}
518 lowers with an increase in convective strength from shallow to deep convection (Muhsin et al.,
519 2018). Under the shallow convection, extreme temperature profiles, in general, show prominent
520 warming (~ 2 K) between 8-14 km due to the latent heat release from convective clouds as a
521 direct response of convection while anomalous cooling (~2 K) just below the CPT and warming
522 (~ 4 K) just above the CPT could be an indirect response to convection (Johnson and Kriete
523 1982; Randel and Wu, 2003). Over the period 2006-2014, there were two tropical cyclones
524 namely Thane and Nilam through Gadanki during 25-31 October 2011 and 28 October - 01
525 November 2012 (Das et al., 2016; Venkat Ratnam et al., 2016). During Nilam cyclone the
526 coldest T_{CPT} (~186 K) on 31 October 2012 was observed over Gadanki.

527 Over Gadanki, Ali et al. (2020) observed that tropopause cirrus warms the CPT by ~ 1.2
528 K which indicates that the extreme tropopause may also result due to radiative effects from the
529 cirrus clouds (Fu et al., 2018; Hartmann et al., 2001). We have used simultaneous observations
530 of the radiosonde and CALIPSO over the same period, however, only two, one, two and three
531 cases are observed for the coldest, warmest, highest and lowest tropopauses, respectively, in the
532 presence of the cirrus clouds indicating that sometimes extreme tropopauses may occur due to
533 cirrus clouds. Finally, we examined the role of the equatorial wave in the occurrence of the
534 extreme tropopauses and found that they can sometimes modify the tropopause structure
535 significantly.

536 The following are the main findings on the extreme variability of the tropical tropopause

1. The probability distribution of the T_{CPT} and H_{CPT} follow nearly Gaussian curve which indicates that 5% of the total behaves extremely with T_{CPT} < 188.5 K, T_{CPT} > 195.9 K, H_{CPT} < 16.5 km and H_{CPT} >17.6 km, defined as the coldest, lowest and highest tropopause, respectively.

2. The extreme tropopauses are distributed throughout the season and occur randomly in all the seasons. The coldest and highest tropopauses occur independently (i.e., the coldest tropopause is not the highest one and vice versa). Similarly, the warmest and lowest tropopauses also occur independently except for a few cases.

3. The occurrence of the extreme tropopauses shows the seasonal variation with minimum occurrence during NH winter and maximum occurrence during NH summer season.

4. The T_{CPT} and H_{CPT} for the extreme cases show similar seasonal variation as the climatological mean T_{CPT} and H_{CPT}, respectively. However, the T_{CPT} of the coldest (warmest) case is always colder (warmer) by about 4-5 K from the climatological mean tropopause throughout the season. The H_{CPT} for the highest (lowest) case is higher (lower) by ~ 1.0 - 1.7 km (~ 1.0 - 1.3 km) from the climatological mean tropopause.

5. The individual extreme temperature profiles under different extreme cases possess similar thermal structures. For the coldest cases, the tropopauses are sharper while rest of other cases is border. These broader tropopauses cases are different among themselves. For the warmest, highest and lowest tropopause cases the temperature between ~16 km to 18.5 km is nearly constant ($\frac{dT}{dz} \cong 0$), slightly decreases ($\frac{dT}{dz} < 0$) and gradually increases ($\frac{dT}{dz} > 0$), respectively.

6. The water vapor profiles and their corresponding mean between pressure levels 130 hPa to 60 hPa each extreme tropopause cases are similar and showing a large variability with

maximum (minimum) water vapor for the warmest (coldest) tropopause cases. Ozone concentrations for the warmest tropopauses are found to be more when compared to the coldest tropopauses.

7. Convection plays an important role in the occurrence of the extreme tropopause cases, especially for the coldest tropopause. Under very shallow convective clouds (H_{CCT} = 2 – 5 km), extreme T_{CPT} though does not show any significant change relative to clear sky condition. For the shallow convective clouds (H_{CCT} = 5 – 8 km), coldest tropopause becomes warmer by ~ 1.5 K and lower by ~0.5 km relative to clear sky condition.

Acknowledgments

This work is fully supported by the Department of Science and Technology, Government of India – Science and Engineering Research Board (DST-SERB) project (EMR/2015/000525). SKM wishes to thank Director, NARL Gadanki, for providing the radiosonde data. The radiosonde data used in this study are available from the dropdown "View & Download Data" listed on the "Data/Experiment" tab of the NARL website (www.narl.gov.in). IRBT data can be obtained from NASA Goddard Earth Sciences Data and Information Services Center (GES DISC). We thank NASA GES DISC for providing Aura-MLS data which can be downloaded from https://disc.gsfc.nasa.gov/datasets

References

Ali, S., Mehta, S. K., Annamalai, V., Ananthavel, A., & Reddy, R. (2020). Qualitative observations of the cirrus clouds effect on the thermal structure of the tropical tropopause. *Journal of Atmospheric and Solar-Terrestrial Physics, 211*, 105440.

Añel, J. A., Antuña, J. C., de la Torre, L., Castanheira, J. M., & Gimeno, L. (2008). Climatological features of global multiple tropopause events. *Journal of Geophysical Research: Atmospheres, 113*(D7).

584 Boehm, M. T., & Verlinde, J. (2000). Stratospheric influence on upper tropospheric tropical cirrus. *Geophysical*
585 *Research Letters, 27*(19), 3209-3212.
586 Borsche, M., Kirchengast, G., & Foelsche, U. (2007). Tropical tropopause climatology as observed with radio
587 occultation measurements from CHAMP compared to ECMWF and NCEP analyses. *Geophysical Research*
588 *Letters, 34*(3).
589 Brewer, A. (1949). Evidence for a world circulation provided by the measurements of helium and water vapour
590 distribution in the stratosphere. *Quarterly Journal of the Royal Meteorological Society, 75*(326), 351-363.
591 Das, S. S., Venkat Ratnam, M., Uma, K., Patra, A., Subrahmanyam, K., Girach, I., et al. (2016). Stratospheric
592 intrusion into the troposphere during the tropical cyclone Nilam (2012). *Quarterly Journal of the Royal*
593 *Meteorological Society, 142*(698), 2168-2179.
594 Dobson, G., Brewer, A., & Cwilong, B. (1946). Meteorology of the lower stratosphere. *Proceedings of the Royal*
595 *Society of Medicine, 185*(Ser A), 144.
596 Fu, Q., Smith, M., & Yang, Q. (2018). The impact of cloud radiative effects on the tropical tropopause layer
597 temperatures. *Atmosphere, 9*(10), 377.
598 Fueglistaler, S., Dessler, A., Dunkerton, T., Folkins, I., Fu, Q., & Mote, P. W. (2009). Tropical tropopause layer.
599 *Reviews of Geophysics, 47*(1).
600 Fueglistaler, S., & Haynes, P. (2005). Control of interannual and longer-term variability of stratospheric water
601 vapor. *Journal of Geophysical Research: Atmospheres, 110*(D24).
602 Gettelman, A., & Birner, T. (2007). Insights into tropical tropopause layer processes using global models. *Journal of*
603 *Geophysical Research: Atmospheres, 112*(D23).
604 Gettelman, A., Hegglin, M. I., Son, S. W., Kim, J., Fujiwara, M., Birner, T., et al. (2010). Multimodel assessment of
605 the upper troposphere and lower stratosphere: Tropics and global trends. *Journal of Geophysical Research:*
606 *Atmospheres, 115*(D3).
607 Hartmann, D. L., Holton, J. R., & Fu, Q. (2001). The heat balance of the tropical tropopause, cirrus, and
608 stratospheric dehydration. *Geophysical Research Letters, 28*(10), 1969-1972.
609 Highwood, E., & Hoskins, B. (1998). The tropical tropopause. *Quarterly Journal of the Royal Meteorological*
610 *Society, 124*(549), 1579-1604.
611 Holton, J. R. (1982). The role of gravity wave induced drag and diffusion in the momentum budget of the
612 mesosphere. *Journal of Atmospheric Sciences, 39*(4), 791-799.
613 Holton, J. R., Haynes, P. H., McIntyre, M. E., Douglass, A. R., Rood, R. B., & Pfister, L. (1995). Stratosphere-
614 troposphere exchange. *Reviews of Geophysics, 33*(4), 403-439.
615 Houze Jr, R. A. (2004). Mesoscale convective systems. *Reviews of Geophysics, 42*(4).
616 Jain, A., Das, S. S., Mandal, T. K., & Mitra, A. (2006). Observations of extremely low tropopause temperature over
617 the Indian tropical region during monsoon and postmonsoon months: Possible implications. *Journal of*
618 *Geophysical Research: Atmospheres, 111*(D7).
619 Jain, A., Panwar, V., Johny, C., Mandal, T., Rao, V., Gautam, R., & Dhaka, S. (2011). Occurrence of extremely low
620 cold point tropopause temperature during summer monsoon season: ARMEX campaign and CHAMP and
621 COSMIC satellite observations. *Journal of Geophysical Research: Atmospheres, 116*(D3).
622 Johnson, R. H., & Kriete, D. C. (1982). Thermodynamic and circulation characteristics, of winter monsoon tropical
623 mesoscale convection. *Monthly Weather Review, 110*(12), 1898-1911.
624 Kim, H., & Dessler, A. E. (2004). Observations of convective cooling in the tropical tropopause layer in AIRS data.
625 Kim, J., & Son, S.-W. (2012). Tropical cold-point tropopause: Climatology, seasonal cycle, and intraseasonal
626 variability derived from COSMIC GPS radio occultation measurements. *Journal of Climate, 25*(15), 5343-
627 5360.
628 Kumar, K. K. (2006). VHF radar observations of convectively generated gravity waves: Some new insights.
629 *Geophysical Research Letters, 33*(1).
630 Matsuno, T. (1966). Quasi-geostrophic motions in the equatorial area. *Journal of the Meteorological Society of*
631 *Japan. Ser. II, 44*(1), 25-43.
632 Meenu, S., Rajeev, K., Parameswaran, K., & Nair, A. K. M. (2010). Regional distribution of deep clouds and cloud
633 top altitudes over the Indian subcontinent and the surrounding oceans. *Journal of Geophysical Research:*
634 *Atmospheres, 115*(D5).
635 Mehta, S. K., Ratnam Madineni, V., & Krishna Murthy, B. (2010, 2010). *Characteristics of multiple tropopauses in*
636 *the tropics.* Paper presented at the 38th COSPAR Scientific Assembly.
637 Mehta, S. K., Ratnam, M. V., & Krishna Murthy, B. (2011). Multiple tropopauses in the tropics: A cold point
638 approach. *Journal of Geophysical Research: Atmospheres, 116*(D20).

Mehta, S. K., Ratnam, M. V., & Murthy, B. K. (2011). Characteristics of the tropical tropopause over different longitudes. *Journal of Atmospheric and Solar-Terrestrial Physics, 73*(17), 2462--2473.

Mehta, S. K., Ratnam, M. V., & Murthy, B. K. (2013). Characteristics of the multiple tropopauses in the tropics. *Journal of Atmospheric and Solar-Terrestrial Physics, 95*, 78-86.

Muhsin, M., Sunilkumar, S., Ratnam, M. V., Parameswaran, K., Murthy, B. K., & Emmanuel, M. (2018). Effect of convection on the thermal structure of the troposphere and lower stratosphere including the tropical tropopause layer in the South Asian monsoon region. *Journal of Atmospheric and Solar-Terrestrial Physics, 169*, 52-65.

Munchak, L. A., & Pan, L. L. (2014). Separation of the lapse rate and the cold point tropopauses in the tropics and the resulting impact on cloud top-tropopause relationships. *Journal of Geophysical Research: Atmospheres, 119*(13), 7963-7978.

Newell, R. E., & Gould-Stewart, S. (1981). A stratospheric fountain? *Journal of the Atmospheric Sciences, 38*(12), 2789-2796.

Pan, L., Randel, W., Gary, B., Mahoney, M., & Hintsa, E. (2004). Definitions and sharpness of the extratropical tropopause: A trace gas perspective. *Journal of Geophysical Research: Atmospheres, 109*(D23).

Paulik, L. C., & Birner, T. (2012). Quantifying the deep convective temperature signal within the tropical tropopause layer (TTL). *Atmospheric Chemistry & Physics, 12*(24).

Randel, W. J., Wu, F., & Gaffen, D. J. (2000). Interannual variability of the tropical tropopause derived from radiosonde data and NCEP reanalyses. *Journal of Geophysical Research: Atmospheres, 105*(D12), 15509-15523.

Randel, W. J., Wu, F., & Rivera Ríos, W. (2003). Thermal variability of the tropical tropopause region derived from GPS/MET observations. *Journal of Geophysical Research: Atmospheres, 108*(D1), ACL 7-1-ACL 7-12.

Ratnam, M. V., Tsuda, T., Kozu, T., & Mori, S. (2006). Long-term behavior of the Kelvin waves revealed by CHAMP/GPS RO measurements and their effects on the tropopause structure.

Ratnam, M. V., Tsuda, T., Shiotani, M., & Fujiwara, M. (2005). New characteristics of the tropical tropopause revealed by CHAMP/GPS measurements. *Sola, 1*, 185-188.

Reid, G., & Gage, K. (1996). The tropical tropopause over the western Pacific: Wave driving, convection, and the annual cycle. *Journal of Geophysical Research: Atmospheres, 101*(D16), 21233-21241.

Schmidt, T., Wickert, J., Beyerle, G., & Reigber, C. (2004). Tropical tropopause parameters derived from GPS radio occultation measurements with CHAMP. *Journal of Geophysical Research: Atmospheres, 109*(D13).

Seidel, D. J., Ross, R. J., Angell, J. K., & Reid, G. C. (2001). Climatological characteristics of the tropical tropopause as revealed by radiosondes. *Journal of Geophysical Research: Atmospheres, 106*(D8), 7857-7878.

Shepherd, T. G. (2002). Issues in stratosphere-troposphere coupling. *Journal of the Meteorological Society of Japan. Ser. II, 80*(4B), 769-792.

Sherwood, P., de Vries, A. H., Guest, M. F., Schreckenbach, G., Catlow, C. R. A., French, S. A., et al. (2003). QUASI: A general purpose implementation of the QM/MM approach and its application to problems in catalysis. *Journal of Molecular Structure: THEOCHEM, 632*(1-3), 1-28.

Sunilkumar, S., Babu, A., & Parameswaran, K. (2013). Mean structure of the tropical tropopause and its variability over the Indian longitude sector. *Climate dynamics, 40*(5-6), 1125-1140.

Takashima, H., Eguchi, N., & Read, W. (2010). A short-duration cooling event around the tropical tropopause and its effect on water vapor. *Geophysical Research Letters, 37*(20).

Tsuda, T., Murayama, Y., Wiryosumarto, H., Harijono, S. W. B., & Kato, S. (1994). Radiosonde observations of equatorial atmosphere dynamics over Indonesia: 1. Equatorial waves and diurnal tides. *Journal of Geophysical Research: Atmospheres, 99*(D5), 10491-10505.

Venkat Ratnam, M., Ravindra Babu, S., Das, S. S., Basha, G., Krishnamurthy, B., & Venkateswararao, B. (2016). Effect of tropical cyclones on the stratosphere–troposphere exchange observed using satellite observations over the north Indian Ocean. *Atmospheric Chemistry and Physics, 16*(13), 8581-8591.

Webster, P. J., & Stephens, G. L. (1980). Tropical upper-tropospheric extended clouds: Inferences from winter MONEX. *Journal of the Atmospheric Sciences, 37*(7), 1521-1541.